

Partial-measurement-enhanced high-dimensional superdense coding in amplitude damping channel with memory

Xing Xiao(肖兴), Zhipeng Yang(杨志鹏), Yan-Ling Li(李艳玲), Fangqing Tang(唐方清), and Tian-Xiang Lu(卢天祥)
Citation: Chin. Phys. B, 2026, 35 (**4**): 040301. DOI: 10.1088/1674-1056/ae27b4
http://cpb.iphy.ac.cn; http://iopscience.iop.org/cpb

What follows is a list of articles you may be interested in

Computing the ground state solution of Bose-Einstein condensates by an energy-minimizing normalized residual network

Ren-Tao Wu(吴任涛), Ji-Dong Gao(高济东), Yu-Han Wang(王宇晗), Zhen-Wei Deng(邓振威), Ming-Jun Li(李明军), and Rong-Pei Zhang(张荣培)
Chin. Phys. B, 2025, 34 (**10**): 100305. DOI: 10.1088/1674-1056/ade062

Coherence migration in high-dimensional bipartite systems

Zhi-Yong Ding(丁智勇), Pan-Feng Zhou(周攀峰), Xiao-Gang Fan(范小刚),Cheng-Cheng Liu(刘程程), Juan He(何娟), and Liu Ye(叶柳)
Chin. Phys. B, 2022, 31 (**6**): 060308. DOI: 10.1088/1674-1056/ac48f8

Controlled unknown quantum operations on hybrid systems

Yong He(何勇), Ming-Xing Luo(罗明星)
Chin. Phys. B, 2016, 25 (**12**): 120304. DOI: 10.1088/1674-1056/25/12/120304

Controlled remote implementation of quantum operations with high-dimensional systems

Zhan You-Bang (詹佑邦), Li Xiao-Wei (李晓薇), Ma Peng-Cheng (马鹏程), Shi Jin (施锦)
Chin. Phys. B, 2013, 22 (**4**): 040306. DOI: 10.1088/1674-1056/22/4/040306

SPECIAL TOPIC — Quantum communication and quantum network

Partial-measurement-enhanced high-dimensional superdense coding in amplitude damping channel with memory

Xing Xiao(肖兴)[1], Zhipeng Yang(杨志鹏)[1], Yan-Ling Li(李艳玲)[2,3], Fangqing Tang(唐方清)[1], and Tian-Xiang Lu(卢天祥)[1,†]

[1] *School of Physics and Electronic Information, Gannan Normal University, Ganzhou* 341000, *China*
[2] *School of Information Engineering, Jiangxi University of Science and Technology, Ganzhou* 341000, *China*
[3] *Jiangxi Provincial Key Laboratory of Multidimensional Intelligent Perception and Control, Jiangxi University of Science and Technology, Ganzhou* 341000, *China*

(Received 25 September 2025; revised manuscript received 20 November 2025; accepted manuscript online 4 December 2025)

We study the performance of high-dimensional superdense coding (HD-SDC) over an amplitude damping (AD) channel with memory and propose a protocol that leverages partial measurement and its reversal to enhance the channel capacity. By considering a two-qutrit system, we model the memory AD noise using a convex mixture of memoryless and perfectly memory AD channels. We demonstrate that the memory effect alone can mitigate the decay of the SDC capacity under noise. More significantly, we show that the application of partial measurement before the channel and its reversal after the channel can not only recover the capacity degraded by noise but, for certain non-maximally entangled initial states, even amplify it beyond the initial capacity. This amplification effect is governed by three key factors: the ground-state probability in the initial entangled state, the memory strength, and the partial measurement strength. Our results provide a practical strategy for enhancing quantum communication protocols in realistic noisy environments and highlight the synergistic benefits of memory noise and measurement-based control.

Keywords: high-dimensional systems, superdense coding, memory noise, partial measurement

PACS: 03.67.–a, 42.50.Lc

DOI: 10.1088/1674-1056/ae27b4 **CSTR:** 32038.14.CPB.ae27b4

1. Introduction

The pursuit of higher information capacity is a fundamental goal in quantum communication.[1–4] While superdense coding (SDC) allows a sender (Alice) to transmit two classical bits by sending a single qubit to a receiver (Bob) with whom she shares a maximally entangled state,[5,6] this protocol can be generalized to higher-dimensional systems. High-dimensional superdense coding (HD-SDC), which utilizes quantum d-dimensional systems (qudits), offers a superior channel capacity of up to $2\log_2 d$ classical bits per transferred qudit.[7–9] This not only improves information capacity but also promises enhanced resistance to noise and increased security in quantum cryptographic applications. As a result, HD-SDC has attracted growing interest as a route to higher-rate quantum communications and denser encoding strategies that exploit larger local Hilbert spaces. The experimental realization of HD-SDC using various degrees of freedom,[7,9] such as the orbital angular momentum of photons, has solidified its potential as a key protocol in the future quantum internet.[10–12]

However, the practical implementation of any quantum communication protocol, including HD-SDC, is inevitably susceptible to noise arising from interactions with the environment.[13] The amplitude damping (AD) channel, which models energy relaxation and photon loss, is ubiquitous in optical, atomic, and solid-state platforms, constituting a canonical noise model in quantum information theory.[14] This noise degrades quantum entanglement, which is a crucial resource for state discrimination, leading to significant deterioration in channel capacity. In certain scenarios, the capacity of HD-SDC in the presence of noise may even fall below that of its classical counterpart, specifically to values less than $\log_2 d$. Consequently, developing strategies to mitigate the detrimental effects of noise is essential for realizing robust and reliable quantum communication.

Most theoretical treatments of quantum noise have relied on the Markovian approximation, in which each channel use interacts with an environment that has no memory and successive uses are independent. While this is a convenient and often reasonable assumption, it fails to capture many realistic scenarios in which the environment exhibits prolonged correlation times (for example, high-Q waveguides, structured reservoirs, or repeated use of the same physical channel at high rate). Quantum channels with memory — where noise influences on successive channel uses are correlated — constitute a significant class of non-Markovian models. These

†Corresponding author. E-mail: lu.tianxiang@foxmail.com

© 2026 Chinese Physical Society and IOP Publishing Ltd. All rights, including for text and data mining, AI training, and similar technologies, are reserved.

models have been demonstrated to exhibit qualitatively different behaviors compared to memoryless channels. In particular, correlations in the noise can lead to nontrivial effects that may be exploited to enhance quantum information tasks.[15–24] For instance, studies have demonstrated that correlated noise can help preserve entanglement for longer durations,[16,25] enhance the performance of quantum teleportation,[26] and improve precision limits in quantum metrology[27] compared to their purely memoryless counterparts.

Among various techniques developed to mitigate decoherence, partial measurement (also referred to in related contexts as weak measurement), along with its reversal operation, has emerged as a powerful and versatile tool.[28–43] In contrast to projective measurement, which irrevocably collapses a quantum state, a partial measurement probabilistically shifts the state toward a preferred basis state without completely destroying its quantum coherence. A key advantage of this approach is its ability to effectively counteract AD noise. Since AD noise drives a quantum system toward the ground state, a strategically applied partial measurement can preemptively oppose this dissipation, followed by a reversal operation that recovers the original state with high probability.

It is important to contrast the partial-measurement-based approach with other powerful noise-mitigation strategies, most notably entanglement purification (also known as distillation).[44–46] Entanglement purification protocols are designed to distill high-fidelity entangled pairs from a larger ensemble of low-fidelity pairs. Indeed, such protocols constitute a cornerstone for scalable quantum networks and repeater-based communication. However, these methods typically require quantum memory to store multiple state copies and complex non-local entangling operations (such as CNOT gates) between these copies. In contrast to these multi-copy protocols, partial-measurement-based strategies are attractive as a single-copy protection technique. They rely solely on local operations and post-selection (or conditional feedback), rather than demanding the multi-copy resources of entanglement purification or the full machinery of quantum error correction. These partial measurement methods have been experimentally validated in several platforms, including photonic[31,32] and solid-state systems,[28,29] for applications such as maintaining single-qubit coherence[31] and preserving entanglement.[32,35,36] Furthermore, the technique has been successfully deployed to enhance quantum Fisher information,[37] improve the fidelity of quantum teleportation,[40,41] and delay decoherence across a variety of noisy channel models.[47]

In this work, we integrate these directions by examining HD-SDC over an AD channel with memory, and explore how partial measurement and its reversal can enhance the SDC capacity within such correlated noise. Specifically, we model a qutrit AD channel with memory acting on consecutive uses of the same AD channel during the process of SDC and analyze how memory influences the achievable capacity. We then propose a protocol leveraging the synergistic effects of memory and partial measurement. Remarkably, significant capacity enhancement is observed with the assistance of partial measurement and reversal operations.

Notably, we demonstrate that for certain classes of non-maximally entangled states, the combined application of partial measurement and reversal enables capacity amplification under memory AD noise — surpassing the capacity attainable in the noiseless scenario. We reveal that this capacity amplification is influenced by three critical factors: the initial probability of the ground state in the shared entangled state, the strength of memory effect, and the degree of partial measurement applied. We identify specific regimes in which capacity amplification can be achieved and elucidate how the benefits depend on these three factors. These results clarify the interplay between high-dimensional encoding, memory effect, and partial-measurement-based protection, offering concrete strategies for enhancing SDC capacity throughput in near-term noisy quantum communication scenarios.

This paper is organized as follows. In Section 2, we introduce the basic concepts involved in the following discussions, such as HD-SDC, qudit AD channel with memory, partial measurement, and its reversal. In Section 3, we investigate the three-dimensional SDC (3D-SDC) in a memory AD channel. We show that memory effect can enhance the SDC capacity. In Section 4, we display how partial measurement and its reversal improve the SDC capacity further, even amplifying it beyond the noiseless capacity. The experimental feasibility is discussed in Section 5. Finally, we give a brief discussion and summarize our main results in Section 6.

2. Basic concepts

2.1. HD-SDC

SDC was originally introduced for two-level bipartite quantum systems by Bennett and Wiesner,[5] and was later extended beyond two-level systems to higher-dimensional quantum systems.[48–50] The fundamental setup involves Alice and Bob sharing a bipartite entangled state on the Hilbert space $\mathbb{C}^d \otimes \mathbb{C}^d$. Without loss of generality, the protocol leverages an entangled state, such as the generalized Bell state

$$|\psi\rangle_{\mathrm{AB}} = \sum_{k=0}^{d-1} l_k |k\rangle_{\mathrm{A}} \otimes |k\rangle_{\mathrm{B}}, \tag{1}$$

with $\sum_k |l_k|^2 = 1$. To encode classical information, Alice performs a local unitary operation W_i, selected from a set $\{W_i\}$ with a priori probabilities p_i, on her portion of the entangled state. This operation results in an ensemble of states for the

pair of systems that Bob subsequently measures. It transforms the global state into

$$\rho_i = (W_i \otimes \boldsymbol{I}_d)\rho(W_i^\dagger \otimes \boldsymbol{I}_d), \tag{2}$$

with $\rho = |\psi\rangle_{\mathrm{AB}}\langle\psi|$. After performing this operation, Alice transmits her encoded subsystem to Bob. Upon receipt, Bob conducts a joint measurement on the entire $d \times d$-dimensional system to decode the classical information Alice intended to send.

Reference [49] demonstrates that mutually orthogonal unitary transformations applied with equal probabilities achieve the maximum SDC capacity. These transformations are defined as

$$W_{i=(u,v)}|j\rangle = \exp\left(\mathrm{i}\frac{2\pi}{d}uj\right)|j+(v \bmod d)\rangle, \tag{3}$$

where the integers u and v range from 0 to $d-1$, and i denotes the imaginary unit ($\mathrm{i}^2 = -1$). Consequently, we obtain d^2 unitary transformations $\{W_i\}$ for encoding, with $W_0 = \boldsymbol{I}_d$. The ensemble of signal states generated by the unitary transformations described in Eq. (3), each occurring with equal probability $p_i = 1/d^2$, is denoted as ρ^*. The maximum amount of classical information that can be reliably transmitted through this quantum channel is referred to as the SDC capacity. This capacity is defined as the maximum value of the Holevo quantity with respect to $\{W_i, p_i\}$

$$C = S(\bar{\rho}^*) - S(\rho), \tag{4}$$

where $S(\rho) = -\mathrm{Tr}(\rho\log_2\rho)$ denotes the von Neumann entropy, and $\bar{\rho}^* = \sum_{i=0}^{d^2-1}\rho_i/d^2$ is the average density matrix of the ensemble encoded by $\{W_i\}$ with equal probabilities.

The ideal capacity of d-dimensional SDC is $2\log_2 d$, offering a higher fundamental capacity than qubit systems. However, in realistic scenarios, the presence of noise, modeled by a completely positive trace-preserving (CPTP) map $\mathcal{E}$, generally reduces the achievable capacity below the ideal noiseless limit. In this case, the capacity of Eq. (4) becomes

$$C = S(\tilde{\rho}^*) - S\big(\mathcal{E}(\rho)\big), \tag{5}$$

where $\tilde{\rho}^* = \sum_{i=0}^{d^2-1}\mathcal{E}(\rho_i)/d^2$ is the average of the signal ensemble after the action of the channel $\mathcal{E}$.

2.2. Qutrit AD channel with memory

In this work, we consider AD noise acting on consecutively transmitted qutrits. If the time interval between two qutrits passing through the AD channel is shorter than the relaxation time of the channel, the memory effect should be taken into account. Below, we derive the Kraus representation of a qutrit AD channel with memory from the master equation description.

We label the energy eigenbasis of a 3-level system by $\{|0\rangle, |1\rangle, |2\rangle\}$ and take $|0\rangle$ as the ground state. A simple and widely used generalization of the qubit AD channel to a qutrit system assumes that each excited level decays to the ground state $|0\rangle$ with the same decay probability $\Gamma \in [0,1)$ during a single channel use. This model captures the loss of population from excited subspaces into the ground state while discarding inter-level cascades; it is sufficient for many communication tasks and for studying how AD noise degrades entanglement and coding protocols. The Lindblad equation for the single-qutrit AD channel is

$$\dot{\rho} = \sum_{k=1,2}\frac{\Gamma}{2}\big(2\sigma_{0k}\rho\sigma_{k0} - \sigma_{kk}\rho - \rho\sigma_{kk}\big), \tag{6}$$

where $\sigma_{ij} = |i\rangle\langle j|$ is the transition operator between $|i\rangle$ and $|j\rangle$. According to the operator-sum representation $\rho(t) = \sum_i E_i\rho E_i^\dagger$, the Kraus operators are

$$E_0 = |0\rangle\langle 0| + \sqrt{\bar{\eta}}\sum_{k=1}^{2}|k\rangle\langle k|, \quad E_k = \sqrt{\eta}|0\rangle\langle k|, \tag{7}$$

where $\eta = 1-\exp(-\Gamma t)$ and $\bar{\square} = 1-\square$. The completeness relation is $E_0^\dagger E_0 + \sum_{k=1}^{2}E_k^\dagger E_k = \boldsymbol{I}_d$.

If the time interval between two qutrits passing through the AD channel is extremely short, consecutive uses of the channel are almost perfectly correlated. Formally, the evolution can be described by the correlated Lindblad equation for the two-qutrit state ρ_{AB} [23,51]

$$\dot{\rho}_{\mathrm{AB}} = \sum_{i=1,2}\frac{\Gamma}{2}\big(2\sigma_{0i}^{\otimes 2}\rho_{\mathrm{AB}}\sigma_{i0}^{\otimes 2} - \sigma_{ii}^{\otimes 2}\rho_{\mathrm{AB}} - \rho_{\mathrm{AB}}\sigma_{ii}^{\otimes 2}\big), \tag{8}$$

where $\sigma_{ij}^{\otimes 2} = \sigma_{ij}\otimes\sigma_{ij}$. Note that $\rho_{\mathrm{AB}} \in \mathbb{C}^{9\times 9}$ is the total state of two qutrits in the standard basis $\{|m,n\rangle = |3m+n+1\rangle\}$ $(m,n=0,1,2)$. The Kraus operators corresponding to the correlated evolution of the two-qutrit state are given by

$$A_{00} = \left(\begin{array}{c|c|c|c} \boldsymbol{I}_{4\times 4} & \boldsymbol{0}_{4\times 1} & \boldsymbol{0}_{4\times 3} & \boldsymbol{0}_{4\times 1} \\ \hline \boldsymbol{0}_{1\times 4} & \sqrt{\bar{\eta}} & \boldsymbol{0}_{1\times 3} & \boldsymbol{0}_{1\times 1} \\ \hline \boldsymbol{0}_{3\times 4} & \boldsymbol{0}_{3\times 1} & \boldsymbol{I}_{3\times 3} & \boldsymbol{0}_{3\times 1} \\ \hline \boldsymbol{0}_{1\times 4} & \boldsymbol{0}_{1\times 1} & \boldsymbol{0}_{1\times 3} & \sqrt{\bar{\eta}} \end{array}\right),$$

$$A_{11} = \left(\begin{array}{c|c|c} \boldsymbol{0}_{1\times 4} & \sqrt{\eta} & \boldsymbol{0}_{1\times 4} \\ \hline \boldsymbol{0}_{4\times 4} & \boldsymbol{0}_{4\times 1} & \boldsymbol{0}_{4\times 4} \\ \hline \boldsymbol{0}_{4\times 4} & \boldsymbol{0}_{4\times 1} & \boldsymbol{0}_{4\times 4} \end{array}\right),$$

$$A_{22} = \left(\begin{array}{c|c|c} \boldsymbol{0}_{1\times 4} & \boldsymbol{0}_{1\times 4} & \sqrt{\eta} \\ \hline \boldsymbol{0}_{4\times 4} & \boldsymbol{0}_{4\times 4} & \boldsymbol{0}_{4\times 1} \\ \hline \boldsymbol{0}_{4\times 4} & \boldsymbol{0}_{4\times 4} & \boldsymbol{0}_{4\times 1} \end{array}\right), \tag{9}$$

where $\boldsymbol{I}_{n\times n}$ is the n-dimensional identity matrix and $\boldsymbol{0}_{n\times m}$ is the zero matrix of size $n\times m$.

A commonly used discrete-time model of memory assumes that with probability $1-\mu$, two consecutive uses undergo independent single-use noise, and with probability μ, the same error occurs on both systems. Here, $\mu \in [0,1]$ is the

memory parameter: $\mu = 0$ corresponds to memoryless (independent) noise, while $\mu = 1$ corresponds to perfect memory (fully correlated noise).

Using the single-qutrit Kraus operators $\{E_i\}_{i=0}^2$ and the two-qutrit correlated Kraus operators $\{A_{kk}\}_{k=0}^2$ defined above, we can construct the channel map with memory. As assumed in our model, the channel's behavior is a probabilistic mixture of two distinct physical processes:

(i) With probability $1-\mu$, the channel acts as a memoryless (independent) noise channel. The noise on the two qutrits is uncorrelated, and the evolution map is described by the tensor product of the single-qutrit Kraus operators: $\mathcal{E}_{\text{mem-less}}(\rho) = \sum_{i,j=0}^2 (E_i \otimes E_j)\rho(E_i \otimes E_j)^\dagger$.

(ii) With probability μ, the channel acts as a perfect memory channel, where the same error occurs on both systems. This correlated evolution is described by the global two-qutrit Kraus operators: $\mathcal{E}_{\text{mem-full}}(\rho) = \sum_{k=0}^2 A_{kk}\rho A_{kk}^\dagger$.

The total channel map $\mathcal{E}_\mu$ is the convex sum of these two maps, weighted by their respective probabilities. The two-qutrit AD channel with memory is therefore

$$\mathcal{E}_\mu = \bar{\mu} \sum_{i,j=0}^{2} E_{ij}\rho_{\text{AB}}(0)E_{ij}^\dagger + \mu \sum_{k=0}^{2} A_{kk}\rho_{\text{AB}}(0)A_{kk}^\dagger, \tag{10}$$

with $E_{ij} = E_i \otimes E_j$. Note that Eq. (10) provides the basis for analyzing the performance of HD-SDC under an AD channel with memory. The convex-mixture memory model with parameter μ provides a simple and tractable way to include correlations between consecutive uses.

2.3. Partial measurement and its reversal

Partial (or unsharp) measurement is a generalized quantum measurement that interpolates between doing nothing and performing a projective (von Neumann) measurement. It provides a controlled, tunable way to induce partial collapse of the state and is widely used in error suppression, state protection, and quantum metrology.[28–43]

A minimal, two-outcome partial measurement that distinguishes the ground (or any chosen) subspace from the rest is obtained from the projectors

$$P \equiv |0\rangle\langle 0|, \qquad Q \equiv \boldsymbol{I}_d - P = \sum_{k=1}^{d-1} |k\rangle\langle k|. \tag{11}$$

The two measurement operators for outcomes "no click" and "clicks" are

$$M_0 = P + \sqrt{1-p}\, Q, \quad M_1 = \sqrt{p}\, Q, \tag{12}$$

where $p \in [0,1]$ is the measurement strength parameter. Physically, outcome 0 corresponds to no click, which partially preserves coherences inside the excited subspace, while outcome 1 corresponds to definitive clicks projecting onto the excited manifold Q. In the limits $p \to 0$ and $p \to 1$, the measurements become trivial and projective onto $\{P, Q\}$, respectively.

Because M_0 is not unitary, its inverse is generally not a physical Kraus operator. However, one can probabilistically undo M_0 on its support by a second post-selected operation. The corresponding reversal operator can be constructed as

$$M_{\text{R}} = \sqrt{1-p_{\text{r}}}\, P + Q, \tag{13}$$

where p_{r} is the reversal parameter, which satisfies $M_{\text{R}}M_0 = \sqrt{1-p}\,\boldsymbol{I}_d$ when $p_{\text{r}} = p$. Hence, conditioned on obtaining the successful reversal outcome associated with M_{R}, the original state is recovered up to a known global factor in the noiseless situation.

3. The 3D-SDC in AD channel with memory

In the following, we discuss 3D-SDC in an AD channel with memory. Following standard convention in this field, the term "3D" refers to the dimension of the individual qudits, i.e., $d = 3$. The total system shared between Alice and Bob, as shown in Eq. (14), is therefore $3 \otimes 3$-dimensional. We assume that an entangled state is initially prepared by Alice

$$|\psi\rangle_{\text{AB}} = \alpha|00\rangle + \beta|11\rangle + \gamma|22\rangle, \tag{14}$$

with $|\alpha|^2 + |\beta|^2 + |\gamma|^2 = 1$. In the SDC scenario, Alice first establishes shared entanglement with Bob by sending one entangled particle, as illustrated in Fig. 1(a). She then performs a set of unitary operations $\{W_i\}$ on her particle to encode classical information and transmits the encoded particle to Bob. Throughout this process, both entangled particles sequentially traverse the same AD channel, which is modeled using the framework of a memory AD channel.

Substituting $\rho_{\text{AB}}(0) = |\psi\rangle_{\text{AB}}\langle\psi|$ into Eq. (10), we obtain the output state of the two qutrits, denoted by $\rho_{\text{AD}} = \mathcal{E}_\mu[\rho_{\text{AB}}(0)]$. To understand the structure of the final state, we recall the basis mapping $\{|m,n\rangle = |3m+n+1\rangle\}$ with $(m,n = 0,1,2)$. The key components of the initial entangled state are therefore $|00\rangle \leftrightarrow |1\rangle$, $|11\rangle \leftrightarrow |5\rangle$, and $|22\rangle \leftrightarrow |9\rangle$. The non-zero elements of ρ_{AD} can be understood physically as follows: the diagonal terms $\rho_{11}, \rho_{55}, \rho_{99}$ correspond to populations of states $|00\rangle$, $|11\rangle$, and $|22\rangle$, respectively. The off-diagonal terms $\rho_{15}, \rho_{19}, \rho_{59}$ (and their conjugates) represent coherences between these components, which are essential for maintaining 3D-SDC capacity. Other terms (e.g., ρ_{22}, ρ_{33}) represent population "leaked" via decoherence into other basis states (such as $|01\rangle$ and $|02\rangle$), primarily induced by the uncorrelated part of the noise. Explicitly, the non-zero elements of ρ_{AD} are

$$\begin{aligned}
\rho_{11} &= |\alpha|^2 + |\beta|^2(\bar{\mu}\eta^2 + \mu\eta) + |\gamma|^2(\bar{\mu}\eta^2 + \mu\eta), \\
\rho_{15} &= \rho_{51}^* = \alpha\beta^*(\bar{\mu}\bar{\eta} + \mu\sqrt{\bar{\eta}}),
\end{aligned}$$

$$
\begin{aligned}
\rho_{19} &= \rho_{91}^{*} = \alpha\gamma^{*}\left(\bar{\mu}\bar{\eta} + \mu\sqrt{\bar{\eta}}\right),\\
\rho_{22} &= \rho_{44} = |\beta|^2\bar{\mu}\bar{\eta}\eta,\\
\rho_{33} &= \rho_{77} = |\gamma|^2\bar{\mu}\bar{\eta}\eta,\\
\rho_{55} &= |\beta|^2\left(\bar{\mu}\bar{\eta}^2 + \mu\bar{\eta}\right),\\
\rho_{59} &= \rho_{95}^{*} = \beta\gamma^{*}\left(\bar{\mu}\bar{\eta}^2 + \mu\bar{\eta}\right),\\
\rho_{99} &= |\gamma|^2\left(\bar{\mu}\bar{\eta}^2 + \mu\bar{\eta}\right).
\end{aligned}
\tag{15}
$$

The 3D-SDC capacity, denoted C_{AD}, is evaluated using Eq. (5). Given the complexity of its analytical expression, we rely on numerical results to illustrate the influence of the memory effect. Figure 2 shows C_{AD} as a function of the noise parameter for different memory factors μ. It is observed that C_{AD} decreases as noise increases. Although partial recovery of capacity occurs under certain conditions, it never exceeds the classical limit of $\log_2 3$. Another notable feature, as shown in Fig. 2, is that the memory effect mitigates degradation of the dense coding capacity: higher values of μ correspond to a slower decay of C_{AD}. Moreover, the range of noise values over which quantum advantage is lost — specifically, where C_{AD} falls below the classical threshold — narrows significantly as μ increases, and vanishes in the ideal memory channel scenario.

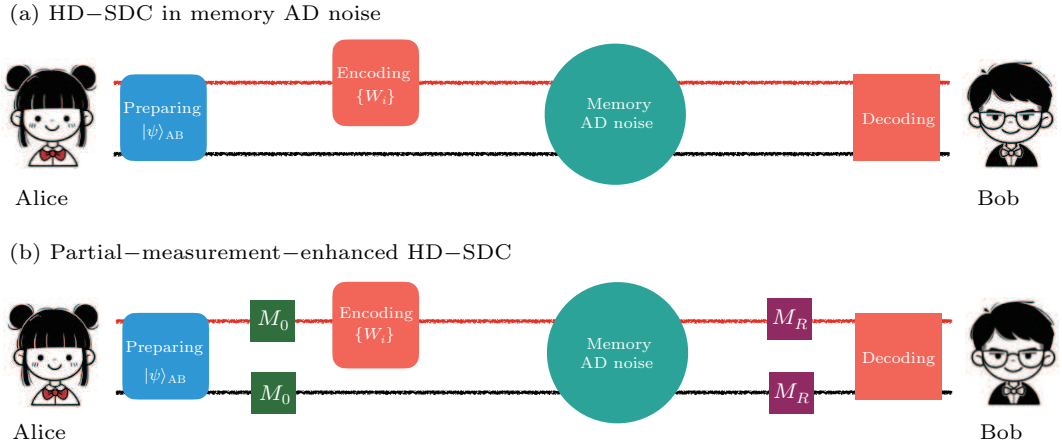


Fig. 1. Schematic illustrations of (a) HD-SDC in a memory AD channel and (b) partial-measurement-enhanced HD-SDC in a memory AD channel. Here, $|\psi\rangle_{\mathrm{AB}}$ denotes the shared entangled state prepared by Alice, while M_0 and M_{R} represent the partial measurement and its reversal, respectively.

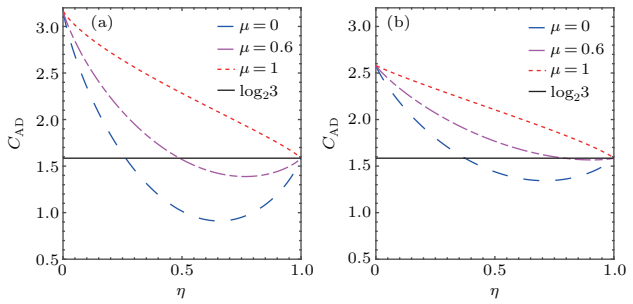


Fig. 2. 3D-SDC capacity C_{AD} as a function of the noise parameter η. Panel (a): $\alpha=\beta=\gamma=\sqrt{1/3}$. Panel (b): $\alpha=\sqrt{7/9}$ and $\beta=\gamma=\sqrt{1/9}$.

4. Enhanced 3D-SDC in AD channel with memory via partial measurement

Based on the aforementioned results, we conclude that the memory effect has the potential to mitigate the decay of capacity. However, it is observed that the quantum advantage progressively diminishes as the noise intensity increases. In this section, we focus on further suppressing noise and enhancing the SDC capacity through the application of partial measurements. Notably, for certain specific initial entangled states, the combined action of the memory effect and partial measurements, together with their reversal operations, can lead to an amplification of the capacity that exceeds the initially noiseless capacity.

4.1. Capacity enhancement

In our scheme, the partial measurement is applied before the noisy channel to partially project the population into a protected subspace, and the reversal operation is applied after the channel to restore the original state probabilistically, as shown in Fig. 1(b). Such a process can be expressed by the following map:

$$
\begin{aligned}
\rho_{\mathrm{PM}} = \frac{1}{\mathcal{N}}\mathbb{M}_{\mathrm{R}}\Bigg[\bar{\mu}\sum_{i,j=0}^{2}E_{ij}\left(\mathbb{M}_{\mathrm{PM}}\rho_{\mathrm{AB}}(0)\mathbb{M}_{\mathrm{PM}}^{\dagger}\right)E_{ij}^{\dagger}\\
+\mu\sum_{k=0}^{2}A_{kk}\left(\mathbb{M}_{\mathrm{PM}}\rho_{\mathrm{AB}}(0)\mathbb{M}_{\mathrm{PM}}^{\dagger}\right)A_{kk}^{\dagger}\Bigg]\mathbb{M}_{\mathrm{R}}^{\dagger},
\end{aligned}
\tag{16}
$$

where $\mathbb{M}_{\mathrm{PM}} = M_0^{\mathrm{A}}\otimes M_0^{\mathrm{B}}$ and $\mathbb{M}_{\mathrm{R}} = M_{\mathrm{R}}^{\mathrm{A}}\otimes M_{\mathrm{R}}^{\mathrm{B}}$.

The resulting state ρ_{PM} has a similar structure, but its elements are now modulated by the partial measurement and reversal parameters. As expected, these parameters act nontrivially on the excited-state components (indices 5 and 9) and their coherences, reflecting the fact that the partial measurement and its reversal operations are designed to protect this subspace from AD noise. For the initial state $|\psi\rangle_{\mathrm{AB}}$, the nonzero elements of the final state ρ_{PM} are

$$
\rho_{11} = \frac{1}{\mathcal{N}}[|\alpha|^2 + (|\beta|^2+|\gamma|^2)(\bar{\mu}\eta^2+\mu\eta)\bar{p}^2]\bar{p}_{\mathrm{r}}^4,
$$

$$
\begin{aligned}
\rho_{15} &= \rho_{51}^{*} = \frac{1}{\mathcal{N}}\alpha\beta^{*}(\bar{\mu}\bar{\eta}+\mu\sqrt{\bar{\eta}})\bar{p}\bar{p}_{\mathrm{r}}^{3},\\
\rho_{19} &= \rho_{91}^{*} = \frac{1}{\mathcal{N}}\alpha\gamma^{*}(\bar{\mu}\bar{\eta}+\mu\sqrt{\bar{\eta}})\bar{p}\bar{p}_{\mathrm{r}}^{3},\\
\rho_{22} &= \rho_{44} = \frac{1}{\mathcal{N}}|\beta|^{2}\bar{\mu}\bar{\eta}\eta\bar{p}^{2}\bar{p}_{\mathrm{r}}^{3},\\
\rho_{33} &= \rho_{77} = \frac{1}{\mathcal{N}}|\gamma|^{2}\bar{\mu}\bar{\eta}\eta\bar{p}^{2}\bar{p}_{\mathrm{r}}^{3},\\
\rho_{55} &= \frac{1}{\mathcal{N}}|\beta|^{2}(\bar{\mu}\bar{\eta}^{2}+\mu\bar{\eta})\bar{p}_{1}^{2}\bar{p}_{\mathrm{r}}^{2},\\
\rho_{59} &= \rho_{95}^{*} = \frac{1}{\mathcal{N}}\beta\gamma^{*}(\bar{\mu}\bar{\eta}^{2}+\mu\bar{\eta})\bar{p}_{1}^{2}\bar{p}_{\mathrm{r}}^{2},\\
\rho_{99} &= \frac{1}{\mathcal{N}}|\gamma|^{2}(\bar{\mu}\bar{\eta}^{2}+\mu\bar{\eta})\bar{p}_{1}^{2}\bar{p}_{\mathrm{r}}^{2},
\end{aligned}
\tag{17}
$$

where $\mathcal{N}=\bar{p}^{4}+\bar{p}^{4}(|\beta|^{2}+|\gamma|^{2})(\bar{\mu}\eta^{2}p_{\mathrm{r}}^{2}-2\eta p_{\mathrm{r}}+\bar{\mu}\eta p_{\mathrm{r}}^{2})$.

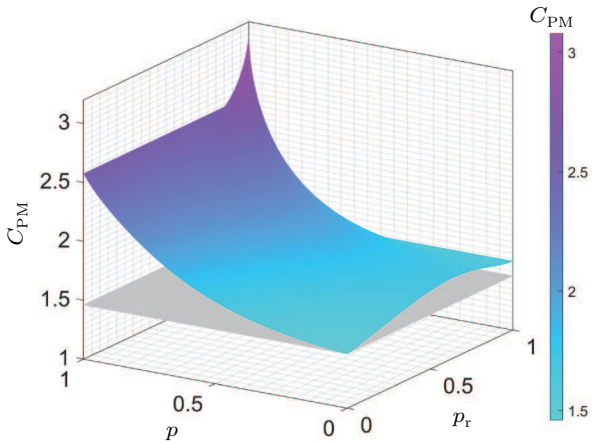


Fig. 3. The capacity C_{PM} (colored surface) as a function of the partial measurement strength p and the reversal measurement strength p_{r}, while the grey plane serves as a reference for the results of C_{AD} (without partial measurement and reversal). The other parameters are $\eta=0.6$, $\mu=0.6$, and $\alpha=\beta=\gamma=\sqrt{1/3}$.

The dense coding capacity C_{PM} of the state ρ_{PM} can be calculated using Eq. (5). Figure 3 shows the variation of C_{PM} with respect to the partial measurement strength p and the reversal measurement strength p_{r} for a fixed parameter $\eta=0.6$. For comparison, we also include the result obtained without partial measurement as a reference. In fact, the result without partial measurement can be obtained by setting $p=p_{\mathrm{r}}=0$. As seen in Fig. 3, the 3D-SDC capacity is enhanced whenever the reversal measurement is applied, even in the absence of partial measurement, i.e., $p=0$ but $p_{\mathrm{r}}\neq 0$. Moreover, the combined use of partial measurement and reversal leads to a further improvement of the capacity.

To achieve the optimal 3D-SDC capacity, it is essential to determine the optimal reversal parameter. Theoretically, the optimal values of p_{r} can be obtained through partial differentiation or numerical simulation. However, the resulting value depends strongly on both the initial state parameters and the memory factor. Given the practical difficulty of precisely determining these quantities in experiments, such an approach is often infeasible. From a physical perspective, we note that the decay processes of both the memoryless AD noise and the perfect memory AD noise can be viewed as quantum transitions, wherein excited states jump to the ground state with certain probabilities. This insight allows us to employ the technique of "unravelling" the dynamics into "jump" and "no-jump" trajectories, thereby enabling effective manipulation of pure states.[32,52] Our approach, therefore, is to identify the most robust, state-independent strategy. The parameter chosen in Eq. (18) is exactly the optimal reversal parameter for the memoryless AD channel. We provide a detailed derivation of this result in Appendix A. Within this framework, the optimal reversal strength yields

$$
p_{\mathrm{r}}^{\mathrm{opt}} = 1-\bar{p}\bar{\eta}. \tag{18}
$$

The distinct advantage of this choice lies in its robustness and state independence. To validate this property, we compare our analytical strategy with the numerically optimized capacity in Fig. 4. Specifically, Fig. 4(a) illustrates the capacity C_{PM} as a function of the noise parameter η (with $p=0.9$), while Fig. 4(b) plots the capacity as a function of the measurement strength p (with $\eta=0.6$). The colored dots represent the full range of achievable capacities obtained by numerically optimizing the reversal parameter p_{r} from 0 to 1, whereas the solid black line corresponds to the capacity determined by our condition Eq. (18). We observe that our physically motivated strategy (black line) closely tracks the true optimal capacity (the upper envelope of the colored dots). This effectively provides near-optimal protection without requiring a priori knowledge of the specific entanglement distribution or the memory parameter. Consequently, in the following discussion, we adopt the reversal operation defined in Eq. (18), and the capacity achieved using this robust, state-independent strategy will be denoted as $C_{\mathrm{PM}}^{\mathrm{opt}}$.

The enhancement of the SDC capacity through partial measurement is demonstrated in Fig. 5. Specifically, Fig. 5(a) shows the influence of the partial measurement strength p and the memory factor μ on the capacities $C_{\mathrm{PM}}^{\mathrm{opt}}$ (upper surface) and C_{AD} (lower surface), while Fig. 5(b) illustrates the effects of the parameter η and the memory factor μ. As evidenced by the plots, the SDC capacity increases monotonically with both p and μ. This behavior can be attributed to the fact that partial measurement effectively mitigates decoherence by selectively projecting the quantum state into a subspace less susceptible to amplitude damping noise. The memory effect further reinforces this protection by correlating noise events, thereby partially preserving quantum correlations and enhancing the capacity. Notably, in the limit of strong partial measurement $p\to 1$, the capacity $C_{\mathrm{PM}}^{\mathrm{opt}}$ approaches its initial value, indicating nearly complete recovery of the original entangled resource. This result highlights the combined role of partial measurement and the memory effect in counteracting decoherence and enhancing the HD-SDC capacity.

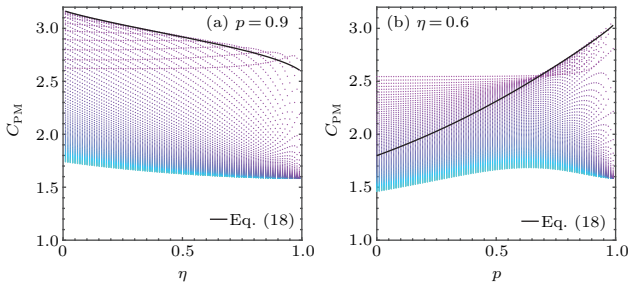


Fig. 4. The capacity $C_{\rm PM}$ (a) as a function of η with $p=0.9$ and (b) as a function of p with $\eta=0.6$, obtained by varying $p_{\rm r}$ from 0 to 1. The black curves denote the results obtained under the condition of Eq. (18). The other parameters are the same as those in Fig. 3.

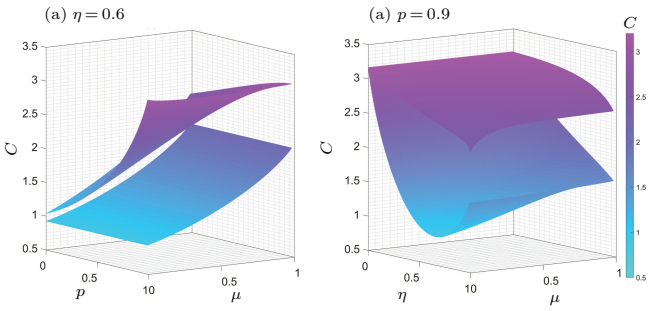


Fig. 5. (a) The capacities $C_{\rm PM}^{\rm opt}$ (upper surface) and $C_{\rm AD}$ (lower surface) as functions of p and μ. (b) The capacities $C_{\rm PM}^{\rm opt}$ (upper surface) and $C_{\rm AD}$ (lower surface) as functions of η and μ. The other parameters are the same as those in Fig. 3.

4.2. Capacity amplification

In the preceding discussion, we found that when the initial shared state is a maximally entangled state, the application of partial measurement techniques can restore the SDC capacity to a value at most equal to that observed in a noise-free scenario, but it cannot exceed this threshold. In the following section, we demonstrate that, for certain non-maximally entangled states, the implementation of partial measurements can lead to capacity amplification in the presence of memory AD noise, thereby enabling the capacity to surpass that of the noise-free case.

In Fig. 6, we plot the SDC capacity $C_{\rm PM}^{\rm opt}$ as a function of the noise parameter η when the initial shared state is a non-maximally entangled state $|\psi\rangle_{\rm AB}=\sqrt{7/9}|00\rangle+\sqrt{1/9}|11\rangle+\sqrt{1/9}|22\rangle$. It is observed that $C_{\rm PM}^{\rm opt}$ increases with the memory factor μ, and notably exceeds the initial value of the capacity — a clear signature of capacity amplification. This amplification can be attributed to the constructive role of memory noise, which partially protects quantum entanglement against decoherence. The protected quantum entanglement is further amplified through partial measurement and reversal. As illustrated in Figs. 6(b) and 6(c), the amplification effect becomes more pronounced with increasing partial measurement strength p. This behavior results from the ability of partial measurement to probabilistically filter out decohered components, thereby effectively concentrating the quantum state into a subspace with higher entanglement. The synergy between the memory effect and partial measurement thus provides a powerful mechanism for enhancing superdense coding performance even in noisy environments.

In order to further determine which initial states can achieve channel capacity amplification and under what circumstances, we define a quantity $\Delta C_{\rm amp}$ to quantify the amplified channel capacity

$$\Delta C_{\rm amp}=C_{\rm PM}^{\rm opt}-C_{\rm AD}(\eta=0), \tag{19}$$

where $C_{\rm AD}(\eta=0)$ denotes the capacity in the noise-free case.

$\Delta C_{\rm amp}$ as a function of α and μ is plotted in Fig. 7. The blank regions represent $\Delta C_{\rm amp}<0$ (without capacity amplification). We observe that the amplification of capacity is influenced by three key factors: first, a stronger memory effect is advantageous; second, a higher strength of partial measurement is beneficial; and third, an increased probability of the ground state in the initial state contributes positively to the capacity amplification. While the influences of the memory effect and partial measurement have been discussed previously, we concentrate here on analyzing the impact of the initial state on capacity amplification.

For the purpose of discussion, we treat α as a free parameter, while setting $\beta=\gamma=\sqrt{(1-\alpha^2)/2}$. Under this assumption, the critical condition for achieving capacity amplification through the memory effect and partial measurement is $\alpha>\sqrt{1/3}$. The stark contrast between the cases $\alpha>\sqrt{1/3}$ and $\alpha<\sqrt{1/3}$ fundamentally stems from their distinct population distributions and the consequent interaction between the measurement and the noise. For the state $|\psi\rangle_{\rm AB}=\sqrt{7/9}|00\rangle+\sqrt{1/9}|11\rangle+\sqrt{1/9}|22\rangle$, the population is highly unbalanced, dominated by the noise-insensitive ground state $|00\rangle$. Here, partial measurement acts as a probabilistic filter that rebalances the population by selectively attenuating the smaller excited-state components. This rebalancing, synergizing with the memory effect which protects the two-qutrit quantum correlations, effectively distills the state into a new configuration with a higher degree of entanglement than the original, thus enabling capacity amplification beyond the initial value. Conversely, for states such as $|\psi\rangle_{\rm AB}=\sqrt{1/9}|00\rangle+\sqrt{4/9}|11\rangle+\sqrt{4/9}|22\rangle$, the population is already favorably distributed in the excited states, which are more fragile to AD noise. In this case, both the noise and the partial measurement act on the same valuable components — the measurement attenuates them, and the noise causes stronger decay. While memory noise can slow the decay, the combined effect of noise and partial measurement is strictly detrimental, making it impossible to exceed the initial capacity. Therefore, the potential for amplification is critically dependent on whether the initial population distribution provides a substrate that partial measurement and the memory effect can optimize rather than degrade.

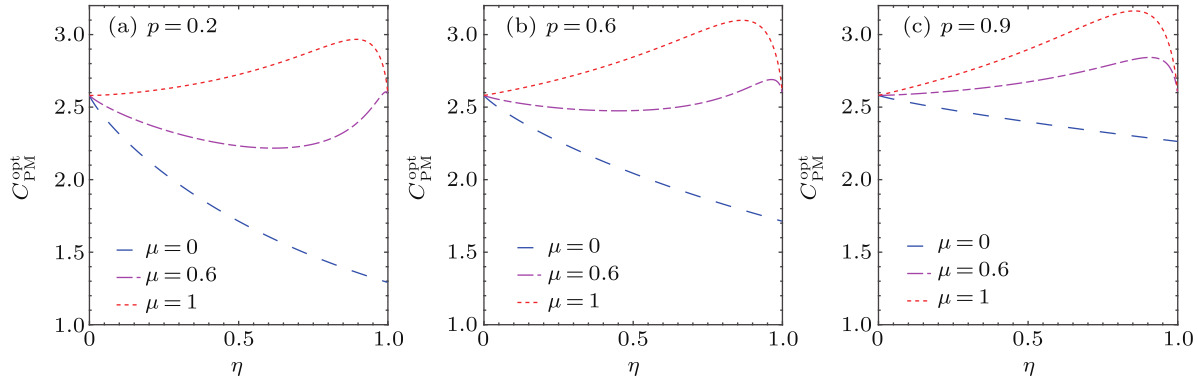


Fig. 6. The capacity $C_{\rm PM}^{\rm opt}$ as a function of the noise parameter η for a non-maximally entangled state $|\psi\rangle_{\rm AB}=\sqrt{7/9}|00\rangle+\sqrt{1/9}|11\rangle+\sqrt{1/9}|22\rangle$. (a) $p=0.2$. (b) $p=0.6$. (c) $p=0.9$.

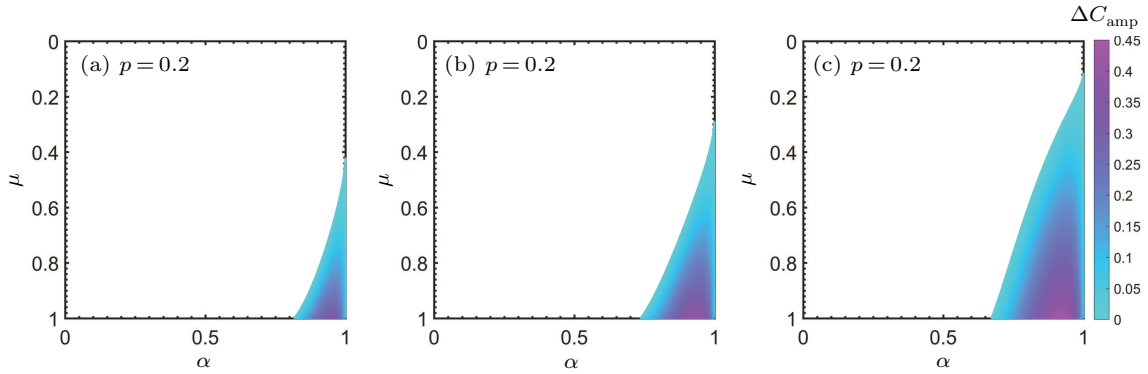


Fig. 7. $\Delta C_{\rm amp}$ as a function of α and μ with $\eta=0.6$. (a) $p=0.2$. (b) $p=0.6$. (c) $p=0.9$. The blank regions represent $\Delta C_{\rm amp}<0$.

4.3. Success probability

Considering that both partial measurement and measurement reversal are non-unitary operations, the present scheme is intrinsically probabilistic. Since the noise channel is trace-preserving, it does not affect the success probability. Hence, the overall success probability is determined by the successful execution of the partial measurement and its reversal in sequence. This can be written as $P_{\rm PM}=\mathcal{P}_1\mathcal{P}_2$, where $\mathcal{P}_1$ and $\mathcal{P}_2$ denote the success probabilities of obtaining the measurement outcomes corresponding to $\mathbb{M}_{\rm PM}$ and $\mathbb{M}_{\rm R}$, respectively

$$P_{\rm PM}=\bar{p}^4+\bar{p}^4(|\beta|^2+|\gamma|^2)\left[\bar{\mu}\eta^2p_{\rm r}^2-2\eta p_{\rm r}+\bar{\mu}\eta p_{\rm r}^2\right]. \quad (20)$$

The success probability $P_{\rm PM}^{\rm opt}$, corresponding to the optimal SDC capacity, is evaluated under the condition specified in Eq. (18). Figures 8(a) and 8(b) show the dependence of $P_{\rm PM}^{\rm opt}$ on the partial measurement strength p and the memory factor μ, respectively.

As illustrated in Fig. 8(a), the success probability decreases monotonically with increasing p. This behavior contrasts with the capacity shown in Fig. 4(b), which increases as p becomes larger. Hence, a trade-off emerges: while a stronger partial measurement enhances the recovery of the SDC capacity, it simultaneously reduces the probability of successfully implementing the protocol.

Conversely, Fig. 8(b) shows that $P_{\rm PM}^{\rm opt}$ increases with the memory factor μ. This indicates that memory noise not only enhances the achievable capacity but also improves the likelihood of successful implementation. Physically, this can be attributed to the fact that noise correlation reduces the entropy of the environment, thereby mitigating the disruptive effects of decoherence and increasing the probability of preserving the quantum state during the partial measurement and reversal process. Consequently, increasing μ is doubly beneficial, as it improves both the capacity and the success probability of the SDC protocol.

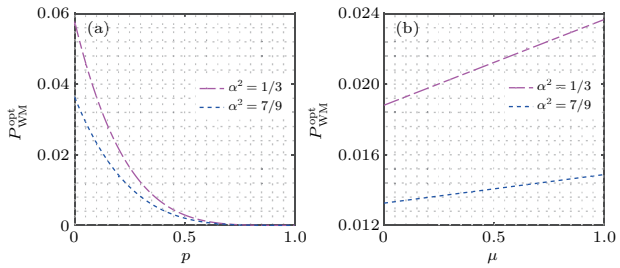


Fig. 8. The success probability $P_{\rm PM}^{\rm opt}$ (a) as a function of p with $\mu=0.6$ and (b) as a function of μ with $p=0.2$. The other parameter is $\eta=0.6$.

5. Experimental feasibility

A concrete test of our scheme is feasible using existing photonic orbital angular momentum (OAM) platforms, which are exceptionally well-suited for high-dimensional quantum information processing.

Step 1: HD-SDC feasibility The realization of HD-SDC, which forms the baseline of our protocol, rests on two criti-

cal components that have already been experimentally demonstrated. (i) HD entanglement: The first requirement is a high-fidelity source of high-dimensional entanglement, which has been successfully achieved in many platforms, including photonics, using OAM.[53–60] (ii) HD Bell-state measurement (BSM): The second, and arguably most challenging, component is the decoding step, which requires a high-dimensional BSM. This is essential for Bob to read out $2\log_2 d$ bits of information, and has also been successfully reported for 3D systems.[53,60] Given that these two cornerstones, a reliable HD entanglement source and a feasible 3D BSM, are available, the standard 3D-SDC protocol itself is well within the reach of current experimental technology.[7]

Step 2: Implementation of partial measurement Our protocol's novel element is the application of partial measurement and its reversal operations (Eqs. (12) and (13)). In the OAM basis, we can make a concrete and feasible proposal: We encode the ground state $|0\rangle$ as the fundamental Gaussian mode ($l = 0$) and the $(d-1)$-dimensional excited subspace Q as the set of all higher-order OAM modes ($l \neq 0$). The key partial measurement operator $M_0 = P + \sqrt{p}Q$ can be physically realized via mode-selective tapping. This requires a custom optical element that can spatially separate the $l = 0$ mode from the $l \neq 0$ modes. For instance, a diffractive phase element or a spatial light modulator (SLM) can be engineered to act as a mode-dependent beam splitter.[7,53,60] This device would have two output paths: (1) Main path: It transmits the $l = 0$ mode (the P subspace) with near-perfect fidelity ($T \approx 1$) (2) Tap path: It reflects a small fraction p of the amplitude from all $l \neq 0$ modes (the Q subspace) into an ancillary detection arm.

A "no-click" in this ancillary detector heralds the successful application of M_0. This event non-destructively attenuates the Q subspace amplitude by the required $\sqrt{1-p}$ exactly as described by the operator, while leaving the P subspace untouched. The reversal operation M_R (Eq. (13)) can be realized in a similar fashion with another post-channel mode-selective element.

Step 3: Simulating the memory AD channel Finally, the AD channel with memory itself can be simulated. A standard optical fiber or free-space propagation acts as a memoryless AD channel. A memory AD channel, where temporal correlations exist, can be engineered by passing the photons through a structured environment, such as a high-Q optical cavity or a coupled multi-core fiber, where the environmental relaxation time is longer than the time separating the two photons.

By integrating the partial measurement-tapping optics (Step 2) into a well-established 3D-SDC setup (Step 1) and employing a memory AD channel (Step 3), our entire scheme is rendered experimentally testable with current technology.

6. Conclusion

In summary, we have investigated the enhancement of HD-SDC capacity in an AD channel with memory through the application of partial measurement and its reversal. We derived the Kraus representation for the qutrit AD channel with memory and analyzed the evolution of the SDC capacity under both memory and partial-measurement-based protection schemes. Our results demonstrate that memory effect alone can enhance the capacity in the presence of noise, and the combined application of partial measurement and its reversal can further increase this capacity, although it does not exceed the capacity achievable in a noise-free scenario.

Notably, we showed that for appropriately chosen non-maximally entangled states, it is possible not only to compensate for noise-induced degradation but also to amplify the capacity beyond its initial noiseless value. This amplification is contingent upon the composition of the initial state, the degree of memory, and the strength of the partial measurement. Furthermore, we discussed the trade-off between capacity enhancement and success probability, noting that while stronger measurements improve capacity, they concurrently reduce the probability of successful outcomes. In contrast, increased memory correlation enhances both the capacity and the success probability.

Finally, we outlined the experimental feasibility of implementing partial measurement in high-dimensional photonic systems through ancillary couplings and mode-selective detection. Theoretically, our scheme can be generalized to arbitrary dimensions ($d > 3$). The underlying physics does not depend on the specific choice of $d = 3$. The partial measurement operators and the AD noise model are already defined for general dimension d. The primary challenges in scaling are not theoretical but experimental and modeling-based. Experimentally, the high-fidelity generation, manipulation, and joint measurement of d-dimensional systems become significantly more complex with increasing d. From a modeling perspective, constructing the explicit correlated Kraus operators for the $d^2 \times d^2$ system is algebraically intensive. However, we emphasize that the specific two-outcome partial measurement we propose (distinguishing $|0\rangle$ from the $(d-1)$-dimensional rest subspace) is far less demanding than a full d-outcome measurement, making our protection strategy fundamentally more scalable than other, more complex measurement-based schemes. Our findings provide valuable insights into the protection and enhancement of quantum communication protocols against decoherence and suggest practical avenues for achieving robust high-rate quantum information transfer in the presence of correlated noise.

Appendix A: Derivation of Eq. (18)

In this appendix, we provide a rigorous justification for the reversal parameter $p_{\mathrm{r}}^{\mathrm{opt}}$ chosen in Eq. (18) of the main text. We show that this parameter is the exact optimal choice for the memoryless AD channel ($\mu = 0$) using the quantum trajectory approach.

Our goal is to find a state-independent reversal parameter p_{r} that maximizes the fidelity of the final state with the initial state, using the trick of "unraveling" the excitation into the "no-jump" trajectory. This is the only trajectory that can, in principle, restore the initial entangled state. For this derivation, we trace the evolution of the "no-jump" component of the initial state $|\psi_{\mathrm{AB}}\rangle = \alpha|00\rangle + \beta|11\rangle + \gamma|22\rangle$.

A1. After partial measurement

The global "no-click" operator is $\mathbb{M}_{\mathrm{PM}} = M_0^{\mathrm{A}} \otimes M_0^{\mathrm{B}}$, which acts as

$$\begin{aligned}
\mathbb{M}_{\mathrm{PM}}|00\rangle &= (P\otimes P)|00\rangle = |00\rangle,\\
\mathbb{M}_{\mathrm{PM}}|11\rangle &= (\sqrt{\overline{p}}Q\otimes\sqrt{\overline{p}}Q)|11\rangle = \overline{p}|11\rangle,\\
\mathbb{M}_{\mathrm{PM}}|22\rangle &= (\sqrt{\overline{p}}Q\otimes\sqrt{\overline{p}}Q)|22\rangle = \overline{p}|22\rangle.
\end{aligned} \tag{A1}$$

The state after a successful measurement (unnormalized) is

$$|\psi_{\mathrm{PM}}\rangle \propto \mathbb{M}_{\mathrm{PM}}|\psi_{\mathrm{AB}}\rangle = \alpha|00\rangle + \beta\overline{p}|11\rangle + \gamma\overline{p}|22\rangle. \tag{A2}$$

A2. After memoryless AD channel (no-jump)

Next, the state evolves through the memoryless AD channel. The "no-jump" part of this evolution corresponds to the Kraus operator $E_{00} = E_0 \otimes E_0$

$$\begin{aligned}
E_{00}|00\rangle &= (P\otimes P)|00\rangle = |00\rangle,\\
E_{00}|11\rangle &= (\sqrt{\overline{\eta}}Q\otimes\sqrt{\overline{\eta}}Q)|11\rangle = \overline{\eta}|11\rangle,\\
E_{00}|22\rangle &= (\sqrt{\overline{\eta}}Q\otimes\sqrt{\overline{\eta}}Q)|22\rangle = \overline{\eta}|22\rangle.
\end{aligned} \tag{A3}$$

The state after the channel, conditioned on zero environmental jumps (unnormalized), is

$$|\psi_{\mathrm{AD}}\rangle \propto E_{00}|\psi_{\mathrm{PM}}\rangle = \alpha|00\rangle + \beta\bar{p}\bar{\eta}|11\rangle + \gamma\bar{p}\bar{\eta}|22\rangle. \tag{A4}$$

A3. After partial measurement reversal

Finally, we apply the global reversal operation $\mathbb{M}_{\mathrm{R}} = M_{\mathrm{R}}^{\mathrm{A}} \otimes M_{\mathrm{R}}^{\mathrm{B}}$

$$\begin{aligned}
\mathbb{M}_{\mathrm{R}}|00\rangle &= (\sqrt{\overline{p}_{\mathrm{r}}}P\otimes\sqrt{\overline{p}_{\mathrm{r}}}P)|00\rangle = \overline{p}_{\mathrm{r}}|00\rangle,\\
\mathbb{M}_{\mathrm{R}}|11\rangle &= (Q\otimes Q)|11\rangle = |11\rangle,\\
\mathbb{M}_{\mathrm{R}}|22\rangle &= (Q\otimes Q)|22\rangle = |22\rangle.
\end{aligned} \tag{A5}$$

The final state for the "no-jump" trajectory is (unnormalized)

$$|\psi_{\mathrm{final}}\rangle \propto \mathbb{M}_{\mathrm{R}}|\psi_{\mathrm{AD}}\rangle = \alpha\overline{p}_{\mathrm{r}}|00\rangle + \beta\bar{p}\bar{\eta}|11\rangle + \gamma\bar{p}\bar{\eta}|22\rangle. \tag{A6}$$

A4. Optimization

To maximize the fidelity, this final state must be proportional to the initial state, i.e., $|\psi_{\mathrm{final}}\rangle \propto |\psi_{\mathrm{AB}}\rangle$. This requires all coefficients to be proportional, which gives the simple, state-independent condition

$$\overline{p}_{\mathrm{r}}^{\mathrm{opt}} = \bar{p}\bar{\eta}. \tag{A7}$$

Substituting the definitions $\overline{p}_{\mathrm{r}} = 1 - p_{\mathrm{r}}$, we solve for the optimal reversal strength $p_{\mathrm{r}}^{\mathrm{opt}}$

$$p_{\mathrm{r}}^{\mathrm{opt}} = 1 - \bar{p}\bar{\eta}. \tag{A8}$$

This is precisely Eq. (18) from the main text. This derivation rigorously proves that our chosen parameter is the exact, state-independent optimal choice that restores the no-jump trajectory for the memoryless AD channel.

Acknowledgments

Project supported by the National Natural Science Foundation of China (Grant Nos. 12265004 and 12534020), the Natural Science Foundation of Jiangxi Province (Grant No. 20242BAB26010), the National Natural Science Foundation of China (Grant Nos. 12565001 and 12205054), the Natural Science Foundation of Jiangxi Province (Grant No. 20252BAC200163), the National Natural Science Foundation of China (Grant No. 12365003), and the Jiangxi Provincial Key Laboratory of Multidimensional Intelligent Perception and Control of China (Grant No. 2024SSY03161).

References

[1] Gisin N and Thew R 2007 *Nat. Photonics* **1** 165
[2] Cariolaro G 2016 *Quantum Communications* (Berlin: Springer)
[3] Orieux A and Diamanti E 2016 *J. Opt.* **18** 083002
[4] Cozzolino D, Da Lio B, Bacco D and Oxenløwe L K 2019 *Adv. Quantum Technol.* **2** 1900038
[5] Bennett C H and Wiesner S J 1992 *Phys. Rev. Lett.* **69** 2881
[6] Barreiro J T, Wei T C and Kwiat P G 2008 *Nat. Phys.* **4** 282
[7] Hu X M, Guo Y, Liu B H, Huang Y F, Li C F and Guo G C 2018 *Sci. Adv.* **4** aat9304
[8] Duan W X and Wang T J 2022 *Phys. Rev. A* **105** 052417
[9] Li Y, Zhu H, Luo W, Cai H, Karim M F, Luo X, Gao F, Wu X, Zhou X, Song Q, Kwek L C and Liu A Q 2025 *npj Quantum Inf.* **11** 49
[10] Kimble H J 2008 *Nature* **453** 1023
[11] Wehner S, Elkouss D and Hanson R 2018 *Science* **362** eaam9288
[12] Cacciapuoti A S, Caleffi M, Tafuri F, Cataliotti F S and Gherardini S 2020 *IEEE Netw.* **34** 137
[13] Brassard G, Nayak A, Tapp A, Touchette D and Unger F 2019 *SIAM J. Comput.* **48** 1147
[14] Nielsen M A and Chuang I L 2010 *Quantum Computation and Quantum Information* (Cambridge: Cambridge University Press)
[15] Macchiavello C and Palma G M 2002 *Phys. Rev. A* **65** 050301
[16] Banaszek K, Dragan A, Wasilewski W and Radzewicz C 2004 *Phys. Rev. Lett.* **92** 257901
[17] D'Arrigo A, Benenti G and Falci G 2007 *New J. Phys.* **9** 310
[18] D'Arrigo A, Benenti G, Falci G and Macchiavello C 2013 *Phys. Rev. A* **88** 042337
[19] von Lüpke U, Beaudoin F, Norris L, Sung Y, Winik R, Qiu J Y, Kjaergaard M, Kim D, Yoder J, Gustavsson S, Viola L and Oliver W 2020 *PRX Quantum* **1** 010305
[20] Lan Y T and Hu M L 2023 *Results Phys.* **54** 107050
[21] Sun Y H and Xie Y X 2022 *Results Phys.* **37** 105526

[22] Li Y L, Liao C H, Yao L and Xiao X 2023 *Results Phys.* **53** 107010
[23] Xu R, Zhou R G, Li Y, Jiang S and Ian H 2022 *EPJ Quantum Technol.* **9** 4
[24] Xing K, Yin A H and Xue Y Q 2024 *Chin. Phys. B* **33** 060309
[25] Ball J, Dragan A and Banaszek K 2004 *Phys. Rev. A* **69** 042324
[26] Yeo Y 2003 *Phys. Rev. A* **67** 054304
[27] Sinclair J, Hallaji M, Steinberg A M, Tollaksen J and Jordan A N 2017 *Phys. Rev. A* **96** 052128
[28] Korotkov A N and Jordan A N 2006 *Phys. Rev. Lett.* **97** 166805
[29] Katz N, Neeley M, Ansmann M, Bialczak R C, Hofheinz M, Lucero E, O'Connell A, Wang H, Cleland A N, Martinis J M and Korotkov A N 2008 *Phys. Rev. Lett.* **101** 200401
[30] Korotkov A N and Keane K 2010 *Phys. Rev. A* **81** 040103
[31] Lee J C, Jeong Y C, Kim Y S and Kim Y H 2011 *Opt. Express* **19** 16309
[32] Kim Y S, Lee J C, Kwon O and Kim Y H 2011 *Nat. Phys.* **8** 117
[33] Xiao X and Li Y L 2013 *Eur. Phys. J. D* **67** 204
[34] Li Y L and Xiao X 2013 *Quantum Inf. Process.* **12** 3067
[35] Man Z X, Xia Y J and An N B 2012 *Phys. Rev. A* **86** 012325
[36] Wang S C, Yu Z W, Zou W J and Wang X B 2014 *Phys. Rev. A* **89** 022318
[37] Xiao X, Yao Y, Zhong W J, Li Y L and Xie Y M 2016 *Phys. Rev. A* **93** 012307
[38] Xiao X, Yao Y, Xie Y M, Wang X H and Li Y L 2016 *Quantum Inf. Process.* **15** 3881
[39] Xiao X, Xie Y M, Yao Y, Li Y L and Wang J 2018 *Ann. Phys.* **390** 83
[40] Xiao X, Yao Y, Li Y L and Xie Y M 2020 *Eur. Phys. J. Plus* **135** 79
[41] Harraz S, Cong S and Nieto J J 2022 *EPJ Quantum Technol.* **9** 15
[42] Metwally N 2016 *EPL* **116** 60006
[43] Behzadi N, Faizi E and Heibati O 2017 *Quantum Inf. Process.* **16** 257
[44] Hu X M, Huang C X, Sheng Y B, Zhou L, Liu B H, Guo Y, Zhang C, Xing W B, Huang Y F, Li C F and Guo G C 2021 *Phys. Rev. Lett.* **126** 010503
[45] Zhou L, Huang C X, Sheng Y B, Guo Y, Hu X M, Huang Y F, Li C F, Guo G C and Liu B H 2025 *Phys. Rev. Lett.* **135** 080501
[46] Luo C C, Gu S P, Wang X F, Zhou L and Sheng Y B 2025 *Chin. Phys. B* **34** 030307
[47] Wang X W, Yu S, Zhang D Y and Oh C H 2016 *Sci. Rep.* **6** 22408
[48] Hausladen P, Jozsa R, Schumacher B, Westmoreland M and Wootters W K 1996 *Phys. Rev. A* **54** 1869
[49] Hiroshima T 2001 *J. Phys. A: Math. Gen.* **34** 6907
[50] Shadman Z, Kampermann H, Macchiavello C and Bruß D 2010 *New J. Phys.* **12** 073042
[51] Yeo Y and Skeen A 2003 *Phys. Rev. A* **67** 064301
[52] Scully M O and Zubairy M S 1997 *Quantum Optics* (Cambridge: Cambridge University Press)
[53] Luo Y H, Zhong H S, Erhard M, Wang X L, Peng L C, Krenn M, Jiang X, Li L, Liu N L, Lu C Y, Zeilinger A and Pan J W 2019 *Phys. Rev. Lett.* **123** 070505
[54] Qiu X, Guo H and Chen L 2021 arXiv:2112.03764 [quant-ph]
[55] Cabrejo-Ponce M, Luiz A L M, Huber M and Steinlechner F 2023 *Laser Photonics Rev.* **17** 2201010
[56] Cervera-Lierta A, Krenn M, Aspuru-Guzik A and Galda A 2022 *Phys. Rev. Appl.* **17** 024062
[57] Lu L, Xia L, Chen Z, Chen L, Yu T, Tao T, Ma W, Pan Y, Cai X, Lu Y, Zhu S and Ma X S 2020 *npj Quantum Inf.* **6** 1
[58] Ding D-S, Shi B, Shi S, Zhou Z Y, Li Y, Shi B and Guo G 2016 *Light Sci. Appl.* **5** e16157
[59] Hu X M, Xing W B, Liu B H, Huang Y F, Li C F, Guo G C, Erker P and Huber M 2020 *Phys. Rev. Lett.* **125** 090503
[60] Hu X M, Zhang C, Liu B H, Cai Y, Ye X J, Guo Y, Xing W B, Huang C X, Huang Y F, Li C F and Guo G C 2020 *Phys. Rev. Lett.* **125** 230501